Electromagnetically Induced Transparency in Circuit Quantum Electrodynamics with Nested Polariton States

Junling Long,[1,2,*] H. S. Ku,[1] Xian Wu,[1] Xiu Gu,[3] Russell E. Lake,[1] Mustafa Bal,[1] Yu-xi Liu,[3,4] and David P. Pappas[1]
[1]National Institute of Standards and Technology, Boulder, Colorado 80305, USA
[2]Department of Physics, University of Colorado, Boulder, Colorado 80309, USA
[3]Institute of Microelectronics, Tsinghua University, Beijing 100084, China
[4]Tsinghua National Laboratory for Information Science and Technology (TNList), Beijing 100084, China

(Received 27 April 2017; revised manuscript received 31 August 2017; published 23 February 2018)

Quantum networks will enable extraordinary capabilities for communicating and processing quantum information. These networks require a reliable means of storage, retrieval, and manipulation of quantum states at the network nodes. A node receives one or more coherent inputs and sends a conditional output to the next cascaded node in the network through a quantum channel. Here, we demonstrate this basic functionality by using the quantum interference mechanism of electromagnetically induced transparency in a transmon qubit coupled to a superconducting resonator. First, we apply a microwave bias, i.e., drive, to the qubit-cavity system to prepare a Λ-type three-level system of polariton states. Second, we input two interchangeable microwave signals, i.e., a probe tone and a control tone, and observe that transmission of the probe tone is conditional upon the presence of the control tone that switches the state of the device with up to 99.73% transmission extinction. Importantly, our electromagnetically induced transparency scheme uses all dipole allowed transitions. We infer high dark state preparation fidelities of $> 99.39\%$ and negative group velocities of up to -0.52 ± 0.09 km/s based on our data.

DOI: 10.1103/PhysRevLett.120.083602

Controllable interaction between electromagnetic quanta and discrete levels in a quantum system, i.e., light matter interaction, is the key to quantum information storage and processing in a quantum network [1,2]. Consider a three-level atomic system driven by two coherent electromagnetic waves. The destructive interference between the two excitation pathways creates a transparency window for one of the drive fields and switches the system into a "dark state." This phenomenon is called electromagnetically induced transparency (EIT) [3]. Recently, EIT has been harnessed for implementing different building blocks of a quantum network, such as all-optical switches and transistors [4–8], quantum storage devices [9–13], and conditional phase shifters [14–18]. Despite this remarkable success, utilizing EIT and related effects at the single-photon and single-atom level with highly scalable devices is a formidable challenge that prevents realization of a practical quantum network [19]. A promising solution is to extend these techniques to the microwave domain using superconducting quantum circuits that are both scalable and enable deterministic placement of long-lived artificial atoms for the network nodes [20–23].

To this end, three-level superconducting artificial atoms have been used to demonstrate coherent population trapping [24] and Autler-Townes splittings (ATS) [25–31]. However, conclusive evidence of EIT in these simple systems eluded researchers, as it is difficult to find a superconducting quantum system with metastable states and lifetimes that satisfy its stringent requirements [32–35]. Recently, progress has been made in a circuit quantum electrodynamics (QED) system that exploits qubit coupling to a single-mode cavity [36]. In that experiment, one leg of the Λ-type system is dipole forbidden, requiring that it be driven with a two-photon transition. The small photon scattering cross section of this two-photon transition hinders applications such as single-atom quantum memory [37], all-optical switching and routing of a single photon gated by another single photon [5], single photon-photon cross phase modulation [29], and vacuum-induced transparency [38]. On the other hand, high scattering cross sections have been observed in a dipole allowed transition of an artificial atom coupled to a one-dimensional waveguide [39]. Thus, implementing a Λ-type system with all dipole allowed transitions in a circuit QED system is highly desirable for building a quantum network with microwave photons.

In this Letter, we report the first observation of EIT using all dipole allowed transitions in a Λ-type system implemented with a superconducting quantum circuit. Our scheme is based on a theoretical proposal [40] that utilizes polariton states generated with a rf biased two-level system coupled to a resonator. Here, we realized the polariton states in a transmon-cavity system and achieved a metastable state with a long lifetime. Moreover, we were able to tune the polariton states to establish a Λ-type system that can be driven with control and probe fields through dipole

allowed transitions. Note that due to the transmission geometry of our cavity where nominally the signal is transmitted on resonance, the observed experimental signal is actually electromagnetically induced absorption (EIA). However, our EIA and conventional EIT have identical underlying physics of quantum interference. Conventional EIT spectra can be observed if a hanger resonator geometry is used. We retain the nomenclature of quantum optics and use the term "EIT" for the rest of the Letter. From our EIT data, a large transmission extinction (99.73%) of the probe field is observed and high dark state preparation fidelity (>99.39%) is inferred. To our best knowledge, the EIT transmission extinction of 99.73% is the highest one that has been observed to date in the circuit QED system. Our EIT scheme opens up new possibilities for realizing scalable devices that utilize single photons and single atoms for constructing EIT as a building block of a quantum network in the microwave domain.

Our experiment is performed on a device that consists of a concentric transmon capacitively coupled to a $\lambda/2$ microstrip resonator with a coupling strength $g/2\pi = 74$ MHz, as shown in Fig. 1(a). The transmon comprises a single $Al/AlO_x/Al$ Josephson junction shunted by a capacitor consisting of a superconducting island and a surrounding ring. The Josephson junction is fabricated with an overlap technique [41]. The transmon has a resonance frequency $\omega_q/2\pi = 5.648$ GHz between its lowest two levels and an anharmonicity $\alpha/2\pi = 262.5$ MHz. The coherence times are measured to be $T_1 = 35\ \mu$s and $T_2^* = 22.5\ \mu$s. The fundamental mode of the resonator is at $\omega_r/2\pi = 6.485$ GHz with an internal quality factor $Q_i = (1.2 \pm 0.2) \times 10^6$ and a loaded quality factor $Q = 7900$ dominated by the strong coupling to the microwave feedline at the output port.

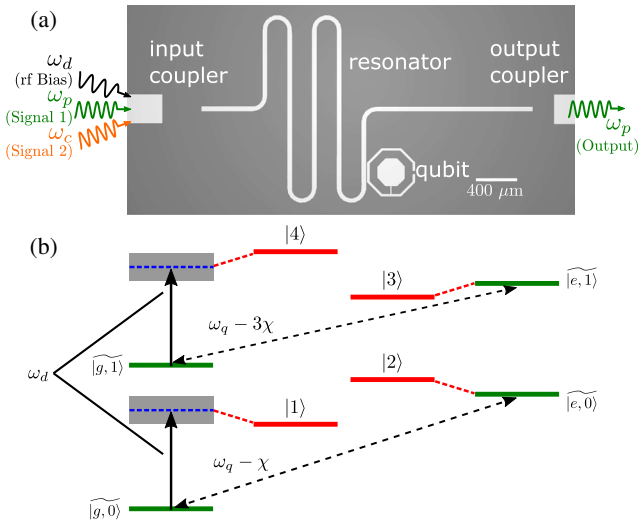

FIG. 1. (a) Optical micrograph (with false color) of the device including a capacitively coupled $\lambda/2$ microstrip resonator and a concentric transmon qubit. ω_d, ω_p, and ω_c are the frequencies of the polariton drive field, the transmission spectrum (or EIT) probe field, and the EIT control field, respectively. (b) Generation of polariton states (red solid lines) in the nesting regime from the Jaynes-Cummings ladder (green solid lines). Black dashed double-headed arrows indicate the photon-number-dependent qubit transitions, black solid arrows show the polariton drive, and the shaded regions denote the nesting regime. ω_q and χ represent the bare qubit frequency and the effective dispersive shift, respectively. Microwave fields are applied through the input coupler in (a).

The transmon-cavity system is well in the dispersive regime with a dispersive shift $\chi/2\pi = 1.54$ MHz. The eigenlevels are described by the dispersive Jaynes-Cummings ladder as shown in Fig. 1(b). The resonance frequencies are $\omega_q - \chi$ for the $|\widetilde{g,0}\rangle \leftrightarrow |\widetilde{e,0}\rangle$ transition and $\omega_q - 3\chi$ for the $|\widetilde{g,1}\rangle \leftrightarrow |\widetilde{e,1}\rangle$ transition, where $|\widetilde{g,n}\rangle$ ($|\widetilde{e,n}\rangle$) denotes the qubit ground (excited) state with n photons in the resonator. The tilde indicates that these levels are singly dressed states; i.e., they are transmon states slightly dressed with resonator photons.

The polariton states are generated by injecting a strong microwave drive field through the input coupler to doubly dress the Jaynes-Cummings states. In particular, if the drive frequency ω_d is in the so-called nesting regime $\omega_q - 3\chi < \omega_d < \omega_q - \chi$, the resulting eigenstates $|2\rangle$ and $|3\rangle$ will be nested in between the eigenstates $|1\rangle$ and $|4\rangle$ [42–44].

We use the set of polariton states $|1\rangle$, $|2\rangle$, and $|3\rangle$ to form a Λ-type system [Fig. 2(d)]. In the driven two-level-system model, these polariton states can be approximated as

$$
\begin{aligned}
|1\rangle &= -\sin\left(\frac{\theta_0}{2}\right)|\widetilde{e,0}\rangle + \cos\left(\frac{\theta_0}{2}\right)|\widetilde{g,0}\rangle,\\
|2\rangle &= \cos\left(\frac{\theta_0}{2}\right)|\widetilde{e,0}\rangle + \sin\left(\frac{\theta_0}{2}\right)|\widetilde{g,0}\rangle,\\
|3\rangle &= -\sin\left(\frac{\theta_1}{2}\right)|\widetilde{g,1}\rangle + \cos\left(\frac{\theta_1}{2}\right)|\widetilde{e,1}\rangle,\\
|4\rangle &= \cos\left(\frac{\theta_1}{2}\right)|\widetilde{g,1}\rangle + \sin\left(\frac{\theta_1}{2}\right)|\widetilde{e,1}\rangle,
\end{aligned}
\tag{1}
$$

where the mixing angles θ_0 and θ_1 are given by $\tan(\theta_0) = \Omega_d/[(\omega_q - \chi) - \omega_d]$ and $\tan(\theta_1) = \Omega_d/[\omega_d - (\omega_q - 3\chi)]$ [40].

Equation (1) shows that the $|1\rangle \leftrightarrow |3\rangle$ and $|2\rangle \leftrightarrow |3\rangle$ transitions are mainly cavitylike transitions, while $|1\rangle \leftrightarrow |2\rangle$ is a qubitlike transition. These properties can be revealed by calculating the decay rate γ_{ij} of the $|i\rangle \rightarrow |j\rangle$ transition, which can be approximated as $\gamma_{31} = \gamma_c \sin^2[(\theta_0 + \theta_1)/2]$, $\gamma_{32} = \gamma_c \cos^2[(\theta_0 + \theta_1)/2]$, and $\gamma_{21} = \gamma_q \cos^4(\theta_0/2)$, where γ_c is the cavity decay rate, and γ_q is the qubit decay rate [40]. Thus, the decay rate of the

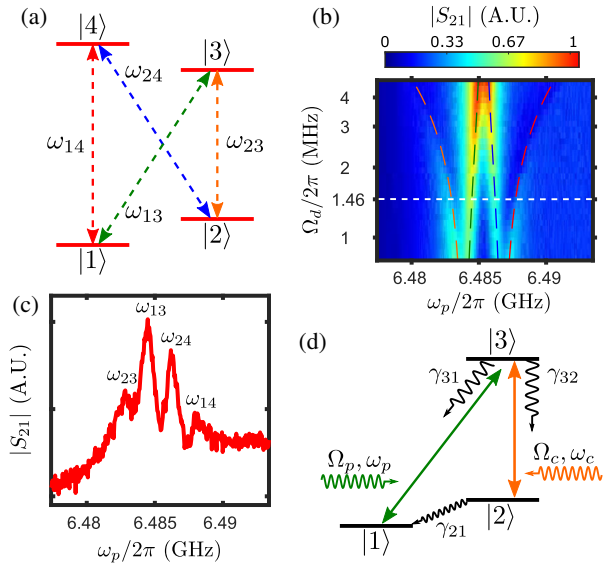

FIG. 2. Transmission spectrum of polariton states in the nesting regime. (a) The four transitions (dashed double-headed arrows) between the polariton states. (b) Transmission spectrum of polariton states in arbitrary units shows the four different transitions in (a). Ω_d and ω_p are the Rabi strength of the polariton drive and the probe frequency, respectively. Dashed curves denote predicted transmission peaks using the ac Stark shift model. (c) A line cut on (b) at $\Omega_d/2\pi = 1.46$ MHz. (d) The lowest three levels $|1\rangle$, $|2\rangle$, and $|3\rangle$ form the Λ-type transition for implementing EIT. Ω_p (Ω_c) and ω_p (ω_c) are the Rabi strength and frequency of the probe (control) field in an EIT experiment, respectively.

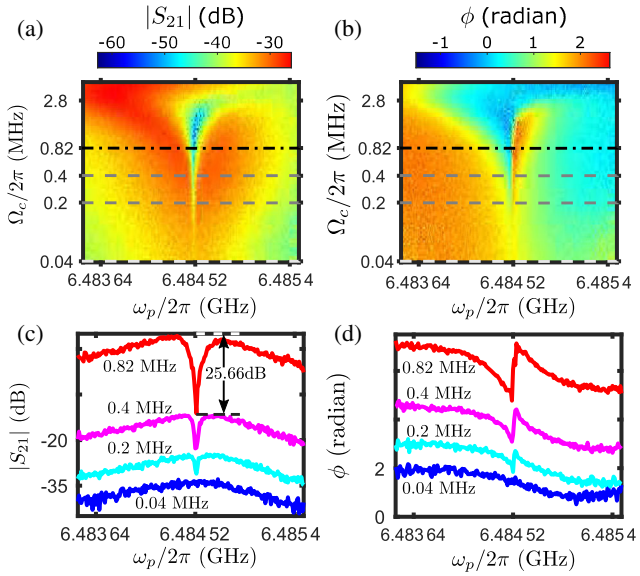

FIG. 3. Transmission magnitude (a) and phase (b) of EIT with varying control field strength. (c) and (d) are line cuts on (a) and (b) with $\Omega_c/2\pi = 0.04$, 0.2, 0.4, and 0.82 MHz, respectively. The black dash-dotted lines in (a) and (b) denote the boundary of EIT set by $\Omega_c/2\pi = \gamma_c/2\pi = 0.82$ MHz. Note that traces are offset vertically from the $\Omega_c/2\pi = 0.04$ MHz case for (c) and (d), and S_{21} data include all round-trip amplification and attenuation.

$|3\rangle \rightarrow |1\rangle$ transition (γ_{31}) can be tuned to be comparable to the decay rate of the $|3\rangle \rightarrow |2\rangle$ transition (γ_{32}), while extending the metastable state lifetime ($1/\gamma_{21}$) even beyond the qubit lifetime. These two effects are key to achieve EIT in our superconducting circuit system.

We measure the transition frequencies between the polariton states by performing two-tone spectroscopy with a polariton drive and a weak probe field. The drive frequency and the probe power are fixed at $\omega_d/2\pi = 5.6466$ GHz and $P_p = -163.15$ dB m, respectively, while scanning the drive strength and the probe frequency. The probe transmission defined as the ratio of the probe output complex amplitude to the input complex amplitude $S_{21} \equiv V_{\text{out}}/V_{\text{in}} = |S_{21}|e^{i\phi}$ was measured by a vector network analyzer (VNA). Our definition of S_{21} includes all round-trip amplification and attenuation, where ϕ has been corrected for electric delay. As shown in Fig. 2(b), there are four transmission peaks near the resonator frequency. The four peaks correspond to, from low to high frequencies, ω_{23}, ω_{13}, ω_{24}, and ω_{14}, respectively [Fig. 2(c)], where ω_{ij} denotes the energy difference between the polariton states $|i\rangle$ and $|j\rangle$. The spacing between the first and second (first and third) transmission peaks, which corresponds to the splitting between levels $|1\rangle$ and $|2\rangle$ ($|3\rangle$ and $|4\rangle$), widens as the drive strength increases. This is consistent with the expected ac Stark shift drawn as the black dashed curves in Fig. 2(b). Another crucial feature of the spectrum is that as the polariton drive strength increases, the height of the ω_{23} and ω_{14} peaks decreases, while the height of the ω_{13} and ω_{24} peaks increases. This behavior agrees with the change of the transition probabilities between the polariton states predicted in Ref. [40].

In this system, EIT is demonstrated by a suppression of transmission for a weak probe field on resonance with one leg of a Λ system, while a control field addressing the other leg [Fig. 2(d)]. The Λ system is established by a polariton drive field with frequency $\omega_d/2\pi = 5.6466$ GHz and strength $\Omega_d/2\pi = 1.46$ MHz. The resultant Λ levels have $\gamma_{31}/2\pi = 0.35$ MHz and $\gamma_{32}/2\pi = 0.47$ MHz, which are much larger than $\gamma_{21}/2\pi = 2.74$ kHz. The control field frequency $\omega_c/2\pi = \omega_{23}/2\pi = 6.4828$ GHz and the probe strength $\Omega_p/2\pi = 62$ kHz are fixed, while we scan the control field strength Ω_c and the probe frequency ω_p. The probe transmission (S_{21}) measured by the VNA is shown in Figs. 3(a) and 3(b). With our parameters, the theoretical condition of EIT is given by $\Omega_c/2\pi < \gamma_c/2\pi = 0.82$ MHz [black dash-dotted line in Fig. 3(a)] [40]. Under this condition, we observe a transmission suppression window around $\omega_p = \omega_{13}$ with the largest suppression 25.66 dB [Figs. 3(c) and 3(d)], which means about 99.73% of the power of the original transmitted probe field is suppressed. However, as the control field strength exceeds the

EIT boundary, the transmission for $\omega_p > \omega_{13}$ in Fig. 3(a) is becoming smaller and completely disappears above $\Omega_c/2\pi = 2.8$ MHz instead of changing to an ATS line shape. This behavior is most likely due to excess cavity population above a single photon, due to the strong control field.

Quantum interferences in a driven Λ system create a dark state, which is transparent to the probe field. The fidelity of the dark state preparation is an important metric for an EIT-based quantum memory [19]. With our experimental parameters, we inferred the dark state fidelity defined as [45]

$$F_{|D\rangle} = \sqrt{\langle D|\rho|D\rangle}, \\ = \sqrt{\frac{1}{2}[\cos 2\Theta(\rho_{11}-\rho_{22}) - \sin 2\Theta(\rho_{21}+\rho_{12}) + (1-\rho_{11})]}, \tag{2}$$

where the dark state $|D\rangle = \cos\Theta|1\rangle - \sin\Theta|2\rangle$ and the mixing angle $\Theta = \tan^{-1}(\Omega_p/\Omega_c)$. The density matrix ρ is calculated by numerically solving a Lindblad master equation of a driven Λ system, including decay rates γ_{ij} [46]. At the EIT boundary ($\Omega_p/2\pi = 0.82$ MHz, $\Omega_c/2\pi = 0$ MHz), the dark state fidelity is calculated to be 99.39%. Note that we switched the role of the probe and the control fields to simulate the fidelity when the dark state is essentially the polariton $|2\rangle$ state and the main infidelity source is its decay rate γ_{21}.

To confirm that the suppression of transmission is due to EIT as opposed to ATS, Akaikes-information-criterion-(AIC) based testing was performed. The AIC-based testing calculates the weight of each fitting model based on the goodness of the fitting with the constraint that the sum of the weights is unity [32]. Originally, the AIC-based testing was proposed to fit the susceptibility χ_s [32]. To use this criterion, we derive the relationship between the measured S_{21} and a generic susceptibility χ_s as [47]

$$\ln(S_{21}) = \ln(|S_{21}|) + i\phi = i\frac{\omega_p L}{c}\left(1+\frac{1}{2}\chi_s\right) - \alpha_0 + i\phi_0, \tag{3}$$

where L is the effective distance the microwave travels through the chip, c is the speed of light, α_0 is the attenuation of the cables, and ϕ_0 is a frequency-independent initial phase offset. For EIT, the susceptibility takes the form of the difference between two Lorentzians [32]

$$\chi_s^{\mathrm{EIT}} = \frac{A_+}{(\omega_p-\omega_+) - i(\Gamma_+/2)} - \frac{A_-}{(\omega_p-\omega_-) - i(\Gamma_-/2)}, \tag{4}$$

and for ATS, it takes the form of the sum

$$\chi_s^{\mathrm{ATS}} = \frac{A_1}{(\omega_p-\omega_1) - i(\Gamma_1/2)} + \frac{A_2}{(\omega_p-\omega_2) - i(\Gamma_2/2)}, \tag{5}$$

where ω_j, A_j, and Γ_j are the center frequency, magnitude, and width of the jth Lorentzian, respectively. In comparison to Ref. [32], the different negative signs in front of the $i(\Gamma_j/2)$ terms in Eqs. (4) and (5) are due to the transmission geometry of the circuit. The model functions for EIT or ATS are then obtained by substituting either χ_s^{EIT} or χ_s^{ATS} for the χ_s in Eq. (3).

We fit the probe transmission S_{21} data to both EIT and ATS models to extract the AIC-based testing weights to validate that the observations were from EIT [32]. For each model, $\ln(|S_{21}|)$ and ϕ were fit simultaneously to assure the Kramers-Kronig relations. The transmission data at $\Omega_c/2\pi = 0.82$ MHz and their fits of both models are shown in Figs. 4(a) and 4(b). Qualitatively, at this control field strength, the data fit significantly better to the EIT

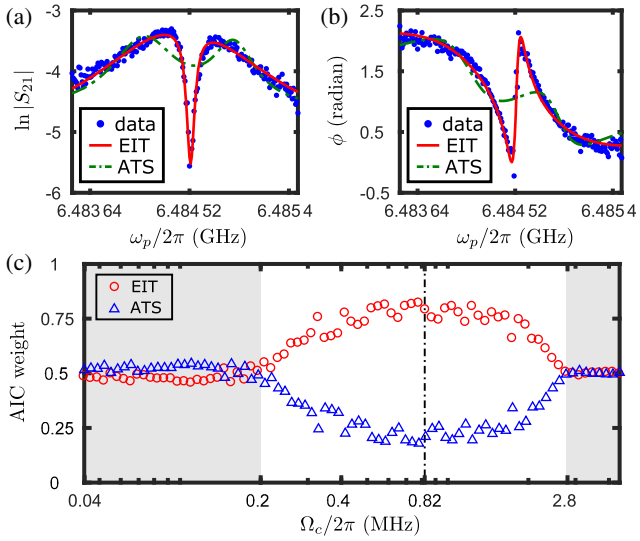

FIG. 4. Fitting the logarithm of transmission magnitude (a) and phase (b) data (blue dots) with the EIT model (red solid curves) and the ATS model (green dash-dotted curves) at $\Omega_c/2\pi = 0.82$ MHz. (c) Calculated weights of EIT and ATS by AIC-based testing. Vertical black dash-dotted line is the EIT boundary given by $\Omega_c/2\pi = \gamma_c/2\pi = 0.82$ MHz. Shaded regions are where both EIT and ATS model fits do not yield meaningful results.

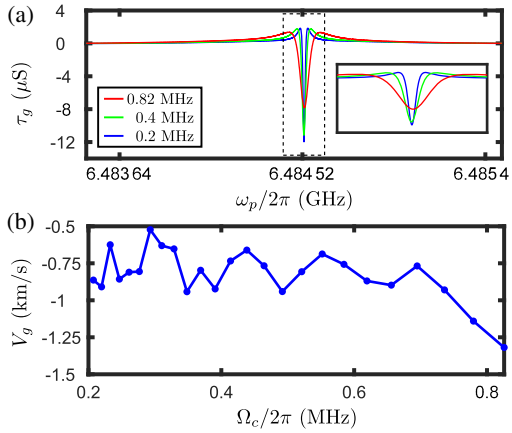

FIG. 5. (a) The time for microwaves to traverse the chip with control field strength $\Omega_c/2\pi = 0.2$, 0.4, and 0.82 MHz. Inset shows an enlarged image of (a) around the center frequency. (b) Calculated group velocity in the center of the transmission suppression window as a function of the control field strength.

model than to the ATS model. Furthermore, the weights of the EIT and ATS models for different control field strengths are plotted in Fig. 4(c). For control field strength $\Omega_c/2\pi < 0.2$ MHz, both the EIT and ATS weights approach 0.5 due to the presence of noise and the relatively small size of transmission suppressions. In the range of 0.2 MHz $< \Omega_c/2\pi <$ 2.8 MHz, the EIT weights are substantially larger than the ATS weights, indicating strong EIT signatures. The maximum EIT weight happens around $\Omega_c/2\pi = 0.82$ MHz, which is in agreement with the theoretical EIT boundary. For control field strength $\Omega_c > 2.8$ MHz, the control field excites resonator photons and drives the system out of the nesting regime. Therefore, there is neither EIT nor ATS characters and results in equal weights of 0.5.

We also investigated the backward light phenomenon due to the giant dispersion of EIT [36]. We calculated the time τ_g for the probe field to traverse the device at different control field strengths by using $\tau_g = -d\phi/d\omega_p$, where ϕ is obtained from the fittings of the EIT model [Fig. 5(a)]. The group velocity of the probe can then be calculated by $v_g = l/\tau_g$, where $l = 10.3$ mm is the distance between the input and output coupler of the device. The largest inferred negative group velocity is $v_g = -0.52 \pm 0.09$ km/s, further pushing the boundaries of slow light, compared to that reported in Ref. [36].

In conclusion, polariton states in the nesting regime were generated with a transmon circuit QED system. The transmission spectra were measured and agree with theoretical predictions. We utilized three levels of nested polariton states to form a Λ-type transition. A robust EIT signature with all dipole allowed transitions was observed in a superconducting system for the first time. Our results constitute an important step toward a scalable quantum network with propagating microwave photons.

X. G. thanks Qi-Chun Liu for discussions. X. G. and Y. X. L. acknowledge the support of the National Basic Research Program of China Grant No. 2014CB921401 and the National Natural Science Foundation of China under Grant No. 91321208. The National Institute of Standards and Technology (NIST) authors acknowledge support of the NIST Quantum Based Metrology Initiative and thank Zachary Dutton for very helpful discussions. This work is the property of the U.S. Government and not subject to copyright.

*Junling.Long@nist.gov

[1] J. I. Cirac, P. Zoller, H. J. Kimble, and H. Mabuchi, Quantum State Transfer and Entanglement Distribution among Distant Nodes in a Quantum Network, Phys. Rev. Lett. **78**, 3221 (1997).
[2] H. J. Kimble, The quantum internet, Nature (London) **453**, 1023 (2008).
[3] M. Fleischhauer, A. Imamoglu, and J. P. Marangos, Electromagnetically induced transparency: Optics in coherent media, Rev. Mod. Phys. **77**, 633 (2005).
[4] S. Baur, D. Tiarks, G. Rempe, and S. Dürr, Single-Photon Switch Based on Rydberg Blockade, Phys. Rev. Lett. **112**, 073901 (2014).
[5] I. Shomroni, S. Rosenblum, Y. Lovsky, O. Bechler, G. Guendelman, and B. Dayan, All-optical routing of single photons by a one-atom switch controlled by a single photon, Science **345**, 903 (2014).
[6] M. Bajcsy, S. Hofferberth, V. Balic, T. Peyronel, M. Hafezi, A. S. Zibrov, V. Vuletic, and M. D. Lukin, Efficient All-Optical Switching Using Slow Light within a Hollow Fiber, Phys. Rev. Lett. **102**, 203902 (2009).
[7] W. Chen, K. M. Beck, R. Bücker, M. Gullans, M. D. Lukin, H. Tanji-Suzuki, and V. Vuletić, All-optical switch and transistor gated by one stored photon, Science **341**, 768 (2013).
[8] J. A. Souza, E. Figueroa, H. Chibani, C. J. Villas-Boas, and G. Rempe, Coherent Control of Quantum Fluctuations Using Cavity Electromagnetically Induced Transparency, Phys. Rev. Lett. **111**, 113602 (2013).
[9] C. Liu, Z. Dutton, C. H. Behroozi, and L. V. Hau, Observation of coherent optical information storage in an atomic medium using halted light pulses, Nature (London) **409**, 490 (2001).
[10] D. F. Phillips, A. Fleischhauer, A. Mair, R. L. Walsworth, and M. D. Lukin, Storage of Light in Atomic Vapor, Phys. Rev. Lett. **86**, 783 (2001).
[11] C. H. van der Wal, M. D. Eisaman, A. André, R. L. Walsworth, D. F. Phillips, A. S. Zibrov, and M. D. Lukin, Atomic memory for correlated photon states, Science **301**, 196 (2003).
[12] A. Kuzmich, W. P. Bowen, A. D. Boozer, A. Boca, C. W. Chou, L.-M. Duan, and H. J. Kimble, Generation of nonclassical photon pairs for scalable quantum communication with atomic ensembles, Nature (London) **423**, 731 (2003).
[13] T. Chaneliere, D. N. Matsukevich, S. D. Jenkins, S.-Y. Lan, T. A. B. Kennedy, and A. Kuzmich, Storage and retrieval of single photons transmitted between remote quantum memories, Nature (London) **438**, 833 (2005).

[14] D. Tiarks, S. Schmidt, G. Rempe, and S. Dürr, Optical π phase shift created with a single-photon pulse, Sci. Adv. **2**, e1600036 (2016).
[15] K. M. Beck, M. Hosseini, Y. Duan, and V. Vuletić, Large conditional single-photon cross-phase modulation, Proc. Natl. Acad. Sci. U.S.A. **113**, 9740 (2016).
[16] E. Shahmoon, G. Kurizki, M. Fleischhauer, and D. Petrosyan, Strongly interacting photons in hollow-core waveguides, Phys. Rev. A **83**, 033806 (2011).
[17] C. Ottaviani, D. Vitali, M. Artoni, F. Cataliotti, and P. Tombesi, Polarization Qubit Phase Gate in Driven Atomic Media, Phys. Rev. Lett. **90**, 197902 (2003).
[18] Z.-Y. Liu, Y.-H. Chen, Y.-C. Chen, H.-Y. Lo, P.-J. Tsai, Ite A. Yu, Y.-C. Chen, and Y.-F. Chen, Large Cross-Phase Modulations at the Few-Photon Level, Phys. Rev. Lett. **117**, 203601 (2016).
[19] L. Ma, O. Slattery, and X. Tang, Optical quantum memory based on electromagnetically induced transparency, J. Opt. **19**, 043001 (2017).
[20] G. Kirchmair, B. Vlastakis, Z. Leghtas, S. E. Nigg, H. Paik, E. Ginossar, M. Mirrahimi, L. Frunzio, S. M. Girvin, and R. J. Schoelkopf, Observation of quantum state collapse and revival due to the single-photon Kerr effect, Nature (London) **495**, 205 (2013).
[21] A. Blais, R.-S. Huang, A. Wallraff, S. M. Girvin, and R. J. Schoelkopf, Cavity quantum electrodynamics for superconducting electrical circuits: An architecture for quantum computation, Phys. Rev. A **69**, 062320 (2004).
[22] D. I. Schuster, A. A. Houck, J. A. Schreier, A. Wallraff, J. M. Gambetta, A. Blais, L. Frunzio, B. Johnson, M. H. Devoret, S. M. Girvin, and R. J. Schoelkopf, Resolving photon number states in a superconducting circuit, Nature (London) **445**, 515 (2007).
[23] J. Koch, T. M. Yu, J. Gambetta, A. A. Houck, D. I. Schuster, J. Majer, A. Blais, M. H. Devoret, S. M. Girvin, and R. J. Schoelkopf, Charge-insensitive qubit design derived from the Cooper pair box, Phys. Rev. A **76**, 042319 (2007).
[24] W. R. Kelly, Z. Dutton, J. Schlafer, B. Mookerji, T. A. Ohki, J. S. Kline, and D. P. Pappas, Direct Observation of Coherent Population Trapping in a Superconducting Artificial Atom, Phys. Rev. Lett. **104**, 163601 (2010).
[25] M. Baur, S. Filipp, R. Bianchetti, J. M. Fink, M. Göppl, L. Steffen, P. J. Leek, A. Blais, and A. Wallraff, Measurement of Autler-Townes and Mollow Transitions in a Strongly Driven Superconducting Qubit, Phys. Rev. Lett. **102**, 243602 (2009).
[26] M. A. Sillanpää, J. Li, K. Cicak, F. Altomare, J. I. Park, R. W. Simmonds, G. S. Paraoanu, and P. J. Hakonen, Autler-Townes Effect in a Superconducting Three-Level System, Phys. Rev. Lett. **103**, 193601 (2009).
[27] A. A. Abdumalikov, O. Astafiev, A. M. Zagoskin, Y. A. Pashkin, Y. Nakamura, and J. S. Tsai, Electromagnetically Induced Transparency on a Single Artificial Atom, Phys. Rev. Lett. **104**, 193601 (2010).
[28] S. Novikov, J. E. Robinson, Z. K. Keane, B. Suri, F. C. Wellstood, and B. S. Palmer, Autler-Townes splitting in a three-dimensional transmon superconducting qubit, Phys. Rev. B **88**, 060503 (2013).
[29] I.-C. Hoi, A. F. Kockum, T. Palomaki, T. M. Stace, B. Fan, L. Tornberg, S. R. Sathyamoorthy, G. Johansson, P. Delsing, and C. M. Wilson, Giant Cross-Kerr Effect for Propagating Microwaves Induced by an Artificial Atom, Phys. Rev. Lett. **111**, 053601 (2013).
[30] B. Suri, Z. K. Keane, R. Ruskov, L. S. Bishop, C. Tahan, S. Novikov, J. E. Robinson, F. C. Wellstood, and B. S. Palmer, Observation of Autler-Townes effect in a dispersively dressed Jaynes-Cummings system, New J. Phys. **15**, 125007 (2013).
[31] S. U. Cho, H. S. Moon, Y.-T. Chough, M.-H. Bae, and N. Kim, Quantum coherence and population transfer in a driven cascade three-level artificial atom, Phys. Rev. A **89**, 053814 (2014).
[32] P. M. Anisimov, J. P. Dowling, and B. C. Sanders, Objectively Discerning Autler-Townes Splitting from Electromagnetically Induced Transparency, Phys. Rev. Lett. **107**, 163604 (2011).
[33] H.-C. Sun, Y.-X. Liu, H. Ian, J. Q. You, E. Il'ichev, and F. Nori, Electromagnetically induced transparency and Autler-Townes splitting in superconducting flux quantum circuits, Phys. Rev. A **89**, 063822 (2014).
[34] B. Peng, S. K. Ozdemir, W. Chen, F. Nori, and L. Yang, What is and what is not electromagnetically induced transparency in whispering-gallery microcavities, Nat. Commun. **5**, 5082 (2014).
[35] Q.-C. Liu, T.-F. Li, X.-Q. Luo, H. Zhao, W. Xiong, Y.-S. Zhang, Z. Chen, J. S. Liu, W. Chen, F. Nori, J. S. Tsai, and J. Q. You, Method for identifying electromagnetically induced transparency in a tunable circuit quantum electrodynamics system, Phys. Rev. A **93**, 053838 (2016).
[36] S. Novikov, T. Sweeney, J. E. Robinson, S. P. Premaratne, B. Suri, F. C. Wellstood, and B. S. Palmer, Raman coherence in a circuit quantum electrodynamics lambda system, Nat. Phys. **12**, 75 (2016).
[37] H. P. Specht, C. Nölleke, A. Reiserer, M. Uphoff, E. Figueroa, S. Ritter, and G. Rempe, A single-atom quantum memory, Nature (London) **473**, 190 (2011).
[38] H. Tanji-Suzuki, W. Chen, R. Landig, J. Simon, and V. Vuletić, Vacuum-induced transparency, Science **333**, 1266 (2011).
[39] O. Astafiev, A. M. Zagoskin, A. A. Abdumalikov, Yu. A. Pashkin, T. Yamamoto, K. Inomata, Y. Nakamura, and J. S. Tsai, Resonance fluorescence of a single artificial atom, Science **327**, 840 (2010).
[40] X. Gu, S.-N. Huai, F. Nori, and Y.-X. Liu, Polariton states in circuit QED for electromagnetically induced transparency, Phys. Rev. A **93**, 063827 (2016).
[41] X. Wu, J. L. Long, H. S. Ku, R. E. Lake, M. Bal, and D. P. Pappas, Overlap junctions for high coherence superconducting qubits, Appl. Phys. Lett. **111**, 032602 (2017).
[42] K. Koshino, K. Inomata, T. Yamamoto, and Y. Nakamura, Implementation of an Impedance-Matched Λ System by Dressed-State Engineering, Phys. Rev. Lett. **111**, 153601 (2013).
[43] K. Inomata, K. Koshino, Z. R. Lin, W. D. Oliver, J. S. Tsai, Y. Nakamura, and T. Yamamoto, Microwave Down-Conversion with an Impedance-Matched Λ System in Driven Circuit QED, Phys. Rev. Lett. **113**, 063604 (2014).
[44] K. Inomata, Z. Lin, K. Koshino, W. D. Oliver, J.-S. Tsai, T. Yamamoto, and Y. Nakamura, Single microwave-photon detector using an artificial Λ-type three-level system, Nat. Commun. **7**, 12303 (2016).

[45] J. Li, G. S. Paraoanu, K. Cicak, F. Altomare, J. I. Park, R. W. Simmonds, M. A. Sillanpää, and P. J. Hakonen, Decoherence, Autler-Townes effect, and dark states in two-tone driving of a three-level superconducting system, Phys. Rev. B **84**, 104527 (2011).

[46] J. R. Johansson, P. D. Nation, and F. Nori, Qutip 2: A python framework for the dynamics of open quantum systems, Comput. Phys. Commun. **184**, 1234 (2013).

[47] J. D. Jackson, *Classical Electrodynamics*, 3rd ed. (Wiley, New York, 1999).